ACS OMEGA

http://pubs.acs.org/journal/acsodf

Article

Time-Domain Observation of Spectral Diffusion in Defective ZnO

Chun Gu,[⊥] Hang Zhang,[⊥] Yonggang Liu, Junhong Yu, Junheng Pan, Guoqiang Luo, Qiang Shen, Jau Tang,* and Jianbo Hu*

Cite This: *ACS Omega* 2021, 6, 15442−15447

Read Online

ACCESS | Metrics & More | Article Recommendations

ABSTRACT: Defects can affect all aspects of materials by altering their electronic structures and mediating the carrier dynamics. However, in the past decades, most research efforts were restricted to nonstoichiometric defects, while the effects of high-density defects on the carrier dynamics of semiconductors remained elusive. In this work, using transient absorption spectroscopy, we have observed for the first time a hybrid carrier relaxation dynamics with the feature of a Poisson-like retard shoulder in a time-domain profile in highly defective ZnO crystals. This novel behavior has been attributed to the spectral diffusion within continuum defect states, which is further confirmed by a proposed diffusion (in energy space) controlled carrier dynamic model. Our results thus reveal an alternative energy decay channel in highly defective crystals and may provide a new route for defect engineering.

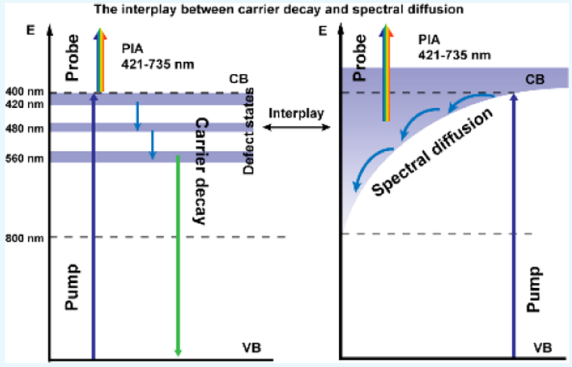

INTRODUCTION

The properties and technological uses of a semiconductor often depend on the defects it contains. The existence of defects and impurities in semiconductors' lattices can dramatically influence their electrical and optical properties.[1] Defect engineering, which involves manipulating the defect type, concentration, and distribution within a semiconductor crystal, has become the primary initiative strategy to design and control the functionality and performance of semiconductor devices.[2,3] By introducing specific types and concentrations of defects in semiconductors, one can obtain the desired semiconductor properties, thus significantly extending their applications to devices.[1,4] On the other hand, for pure and structurally perfect semiconductors, defects are usually unavoidably generated during their natural aging and under extreme working conditions, such as outer space and irradiation environments, severely affecting their originally designed functionality and performance.[5] Therefore, understanding defects' effects has become an inevitable and critical issue for designing, fabricating, and applying semiconductors.

Studying the defect-related carrier dynamics is crucial for gaining the fundamental understanding of how defects affect the semiconductor properties and further optimize the semiconductor devices' performance through defect engineering.[6−9] In the past decades, numerous works have been carried out to improve our understanding of this critical issue. However, one important yet experimentally unexplored question concerning the role of high-density defects (i.e., defect energy band becomes a continuum instead of discrete) in the carrier dynamics, which may be key to further the versatile defect engineering.[7,10,11] Zinc oxide (ZnO) as a wide band gap (3.37 eV) semiconductor has attracted much attention due to promising ultraviolet optoelectronic device applications.[12−15] Native defects in ZnO have long been believed to play a critical role in its optoelectronic performance due to its ability to tune the carrier dynamics, leading to novel properties such as controllable emission from ultraviolet to the yellow range.[7,16−20] Therefore, in this work, taking ZnO as a representative of highly defective semiconductors, we employ transient absorption (TA) spectroscopy to uncover the high-density defect-mediated carrier dynamics. TA experiments observe a novel Poisson-like delayed shoulder in the time-domain profile. We attribute it to the spectral diffusion within continuum defect states, which is further confirmed by a proposed diffusion (in energy space)-controlled carrier dynamic model. Our results thus reveal an alternative energy decay channel in highly defective crystals.

RESULTS AND DISCUSSION

Figure 1b shows the fine-scan absorption spectrum of the sample which exhibits a clear absorption edge at ∼375 nm (3.31 eV) due to the band edge free exciton absorption.

Received: April 10, 2021
Accepted: May 18, 2021
Published: June 1, 2021

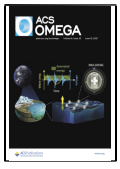

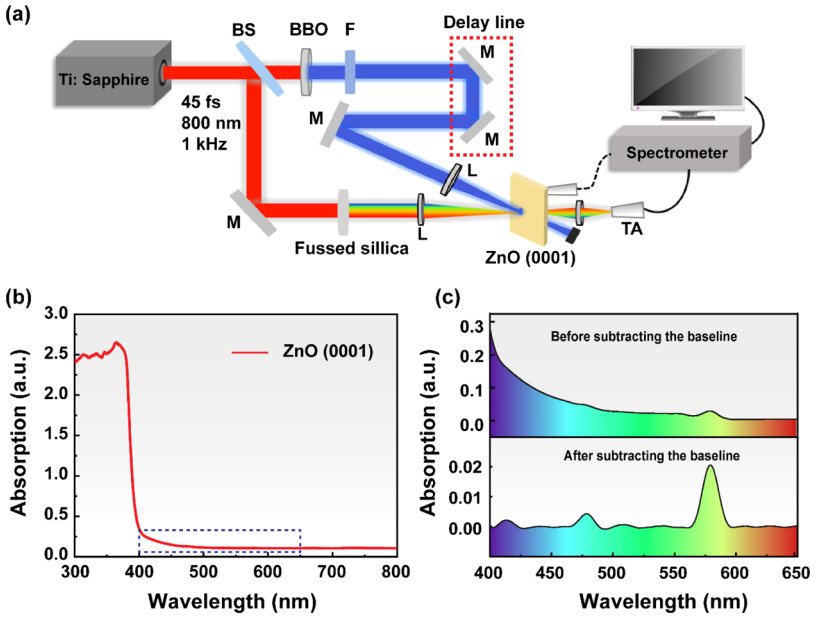

Figure 1. (a) Schematic diagram of the TA spectroscopy setup. BS-beam splitter, BBO-BaB_2O_4 crystal, F-notch filter, M-mirror, and L-lens. (b) Fine-scan UV−vis absorption spectrum of ZnO (0001). (c) Zoomed-in view of absorption in the wavelength range from 400 to 650 nm before and after subtracting the baseline.

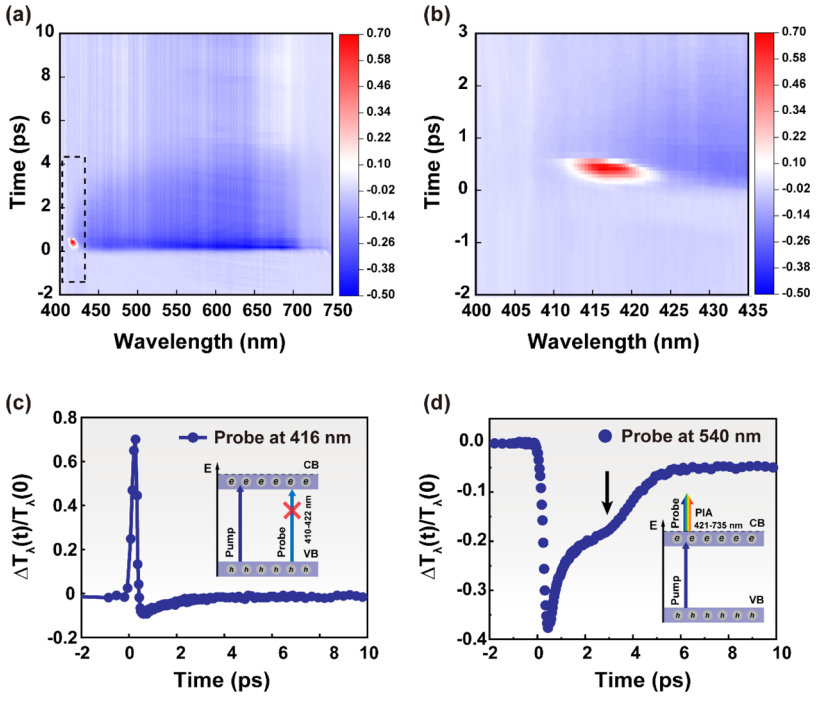

Figure 2. (a) Transient transmission spectra in the wavelength range from 400 to 750 nm. (b) Zoomed-in view spectra in the wavelength range of 410−422 nm, as indicated by a dashed box in (a). Transient transmission trace at the probe wavelengths of 416 nm (c) and 540 nm (d). Insets of (c,d) show schematic diagrams to describe the carrier dynamics.

Besides, an obvious and broad below-band-gap absorption tail in the range of 400−650 nm was observed, indicating the existence of quasi-continuum broad defect states in the band gap.[10,11,19,21−24] By subtracting the exponentially decaying baseline, which corresponds to the quasi-continuum defect states, three discrete peaks located at 2.95 (420 nm), 2.58 (480 nm), and 2.21 eV (560 nm) are visible, as shown in Figure 1c, signifying the coexistence of three denser discrete defect bands and continuum defect states in this highly defective ZnO crystal. It should be noted that these sub-band-gap defect absorption bands observed in Figure 1c are not general features for defective ZnO because different preparation methods, storage environments, and even the degree of aging might cause the diversification of defect types and concentrations, leading to different defect absorption features. However, the broad defect absorption and emission (visible range, especially green for ZnO) phenomenon are not specific but widely found in ZnO crystals which are believed to

https://doi.org/10.1021/acsomega.1c01890
ACS Omega 2021, 6, 15442−15447

originate from the crystalline imperfection of intrinsic defects such as oxygen vacancies (V_O),[25] Zn vacancies (V_{Zn}),[26] Zn interstitials (Zn_i),[27] O antisites (O_{Zn}),[28] and their complexes.[29,30]

Figure 2a shows a typical transient transmission spectrum $\Delta T_\lambda(t)/T_\lambda(0)$ at the excitation fluence of 6.0 mJ/cm^2, in which there exists two distinct regions across the SC wavelength range. The first one, zoom-in shown in Figure 2b, in the wavelength range from 410 to 422 nm, exhibits an enhanced transmitted intensity compared to the equilibrium transmission right after pumping, which is opposite to the second, in the wavelength range from 423 to 725 nm, in which the transmission is reduced.

Typical normalized transient transmission evolutions at specific wavelengths (416 and 540 nm) in these two regions are demonstrated in Figure 2c,d, respectively. In Figure 2c, $\Delta T_\lambda(t)/T_\lambda(0)$ increases after pumping immediately to a maximum and then quickly (<300 fs) falls to a negative value. In principle, the pump-induced transparency effect can be associated with the reduction of optical resonances due to pump-induced bleaching (PIB), schematically shown in the inset of Figure 2c.[7] In this work, after 400 nm pumping, photoexcited electrons relax into the low-lying defect states at 2.9−3.0 eV, thus reducing the absorption of SC probe pulses in the wavelength range of 410−422 nm. The decrease in transmission, on the other hand, arises from the secondary absorption of the SC probe pulses to the conduction band by photoexcited electrons, the so-called pump-induced absorption (PIA), as shown in the inset of Figure 2d.[31] Such a positive to negative conversion suggests a competition between the PIB and PIA effects, which is strongly dependent on the density of the occupied defect states at 2.9−3.0 eV. At the beginning of the excitation, the electron density in these states is relatively high; therefore, the PIB effect dominates over the PIA effect. However, with the electron density decreasing, the PIA effect becomes dominant, turning $\Delta T_\lambda(t)/T_\lambda(0)$ to negative. The sharpness of the conversion indicates a rapid transition of photoexcited carriers among defect states.

More intriguingly, the transmission evolution at λ = 540 nm, as shown in Figure 2d, exhibits a reproducible hybrid relaxation process with a delayed shoulder in the time profile. These featured dynamics are extremely different from the general one in which carriers decay exponentially among discrete energy bands. With only the transitions between states, the resultant multiexponential decay profile could not lead to the shoulder observed here. Actually, such hybrid dynamics often indicate a competitive interplay of more than one process.[32] Keeping that in mind, we can fit the transient transmission evolution using the following empirical equation

$$\frac{\Delta T_\lambda(t)}{T_\lambda(0)} = A_0 + \sum_{i=1}^{2} A_i\left(1 - \exp\left(-\frac{t}{\tau_i}\right)\right) + A_3\left(\frac{t}{\tau_3}\right)^6 \exp\left(-\frac{t}{\tau_3}\right) \quad (1)$$

where A_0 is the offset of the differential transmission and A_i is the amplitude of each component with the lifetime τ_i. The last term represents an empirical Poisson function. By fitting, we numerically decompose the hybrid dynamics into two components as follows: one related to the exponential carrier decay among discrete states and the other related to a Poisson-like process. As shown in Figure 3a (red solid line), eq 1 can be

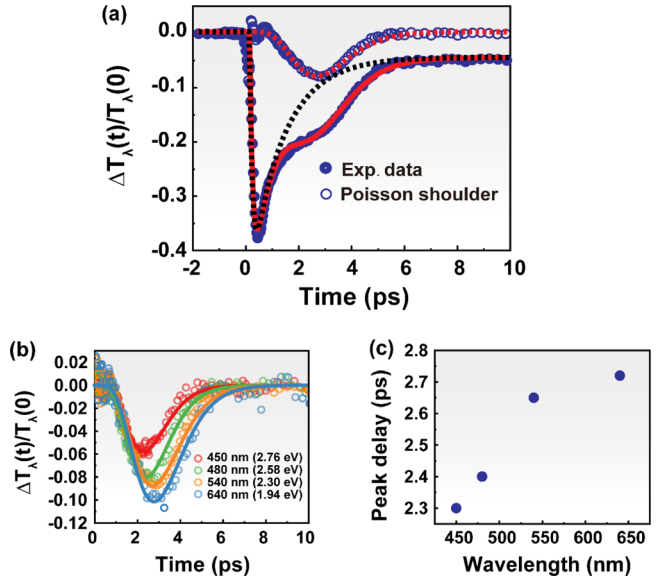

Figure 3. (a) Comprehensive view of the decomposition into biexponential carrier decay (black dashed line) and Poisson-like decay (hollow blue circle) and their numerical fitting. The Poisson-like shoulder is obtained by subtracting the biexponential fit from experimental data. (b) Poisson-like shoulder for the time profile at different probe wavelengths and its numerical fitting. (c) Peak delay time of the Poisson-like shoulder at different probe wavelengths.

used to perfectly fit the experimental result. The contribution of each component is well decomposed. The regular carrier decay (black dashed line) is given by a biexponential function of the time constants of τ_1 = 0.17 ps and τ_2 = 2.5 ps. We attribute this biexponential constant to the average characteristic time of carrier decay among discrete defect states (τ_1 = 0.17 ps) and recombination at a valence band (τ_2 = 2.5 ps), respectively. Such sub-ps to ps defect-related carrier trapping timescale was also observed in the previous research, in which carrier trapping timescale is claimed highly dependent on the density of defects in ZnO crystals.[7]

The decay process showing a Poisson-like time profile (blue circles and red dashed line) reminds us of the energy diffusion in continuum states, which is universal in energy disorder systems such as self-assembled quantum dots and organic molecular materials. In such systems, energy diffusion is the governing mechanism for various processes relating to electron transfer, energy transfer, and fluorescence blinking, in which carriers tend to hop among different energetic sites within a quantum dot or molecules, thus leading to a random spectral shift of the emission line, the so-called spectral diffusion.[33−37] This kind of carrier migration dynamics has been extensively studied by time-resolved methods, and nonexponential dynamic behaviors have been reported.[38,39] Although the ZnO crystal studied here is bulk, the continuum defect band identified by the absorption spectrum may act as different adjacent energy sites for energy diffusion, similar to the energy disorder systems. Photoexcited carriers preferentially hop from the upper level of the continuum defect band (i.e., energy sites at the conduction band edge) to deeper defect sites, exhibiting the Poisson-like process in the time profile.

Figure 3b,c shows the experimental decay time profiles as a result of wavelength-dependent hybrid dynamics. Although the biexponential constant of the carrier decay process among discrete defect bands is nearly independent of the probe

https://doi.org/10.1021/acsomega.1c01890
ACS Omega 2021, 6, 15442−15447

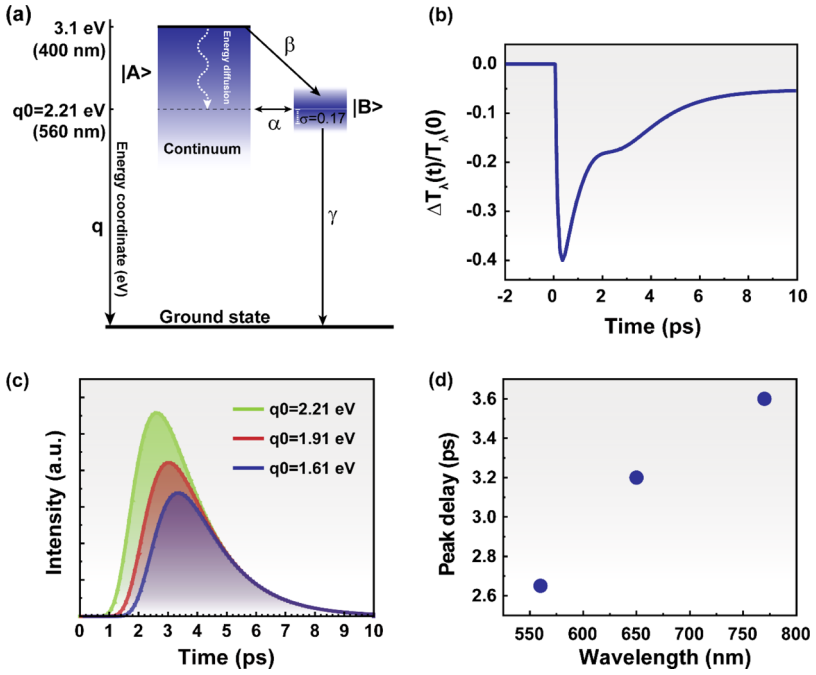

Figure 4. (a) Schematic diagram describing the simplified model of the interplay of carrier decay and energy diffusion in the fuzzy band-edge states. (b) Simulated transient transmission at q_0 = 2.21 eV according to eq 2. (c) Simulated Poisson-shaped delayed time profile at different defect state energy levels. (d) Simulated peak delay times of the Poisson decay at different defect state energy levels.

wavelength (not shown in the text), the energy diffusion in continuum defect states is highly sensitive to the probe sites. With the increasing probe wavelength from 450 to 640 nm, the Poisson-like temporal profile peak shifts from 2.3 to 2.73 ps, which is physically reasonable because it takes time to diffuse from higher energy sites to lower ones.

In order to verify our conjecture, we propose here a model that involves energy diffusion in energy space, as schematically shown in Figure 4a. Based on the observed absorption tail, as shown in Figure 1b, we consider in our model an initial population at the upper edge state of |A> which also includes a lower continuum band representing a fuzzy energy distribution. This initial population of the upper continuum states of |A> has two parallel decay pathways. First, it could decay by energy diffusion into the lower lying continuum states. Besides, it could decay at a rate β to the defect band state |B>, which has a Gaussian-shaped energy distribution with a width of σ (0.17 eV) according to the PL spectrum. The coupling rate between |A> and |B> is given by α. The state |B> can also decay to the ground state at a rate γ. Because the continuum states |A> have a nonuniform density of the state distribution, similar to the electron or energy transfer theories, we consider a parabola potential $U(q)$ in a reaction coordinate q in the energy space with the state |A> lying at the bottom of the parabolic potential. Thus, for nonfree space energy diffusion, the overall rate equation for the population $\rho(q,t)$ in these states and the relevant processes can be given by the following equation

$$\frac{\partial}{\partial t}\rho_A(0,t) = \bar{L}\rho_A(q,t)|_{q=0} - (\rho_A(0,t) - \rho_B(q,t))\frac{\beta}{\sqrt{2\pi}\sigma}\exp\left(-\frac{(q-q_0)^2}{2\sigma^2}\right)$$

$$\frac{\partial}{\partial t}\rho_A(q,t) = \bar{L}\rho_A(q,t) - (\rho_A(q,t) - \rho_B(q,t))\frac{\alpha}{\sqrt{2\pi}\sigma}\exp\left(-\frac{(q-q_0)^2}{2\sigma^2}\right), \text{ for } q \neq 0$$

$$\frac{\partial}{\partial t}\rho_B(q,t) = (\rho_A(q,t) - \rho_B(q,t))\frac{\alpha}{\sqrt{2\pi}\sigma}\exp\left(-\frac{(q-q_0)^2}{2\sigma^2}\right) + (\rho_A(0,t) - \rho_B(q,t))\frac{\beta}{\sqrt{2\pi}\sigma}\exp\left(-\frac{(q-q_0)^2}{2\sigma^2}\right) - \gamma\rho_B(q,t)$$

$$\text{with the initial condition } \rho_A(q,0) = 0 \text{ except } \rho_A(0,0) = 1,\ \rho_B(q,0) = 0 \quad (2)$$

where the Liouville diffusion operator is $\bar{L} = \Delta^2/\tau_c\partial/\partial q[\partial/\partial q + \varsigma/k_BT(q - 3.1)]$, Δ is the energy lattice point. $D = \Delta^2/\tau_c$ is the diffusion coefficient along with the energy coordinate q, and q_0 is the energy for the defect state |B>. The parabolic potential is defined as $U(q) = \varsigma(q - 3.1)^2/2$ where ς is the force constant and 3.1 eV is the band gap of the upper edge of |A>.

We numerically solved eq 2 to calculate the population in time by using the finite difference method. An energy coordinate of about 3.1 eV was divided into 1000 lattice points Δ (3.1×10^{-3} eV). The time evolution was calculated with a time step of 1 fs. The simulated results, as shown in Figure 4b, qualitatively reproduce the overall recovery process observed in the experiments. The Poisson-like energy diffusion process, as presented in Figure 4c,d, is obviously dependent on the probed energy state, which is in good agreement with experimental data (see Figure 3c). It is interesting to note that the energy diffusion coefficient D identified is 1.8×10^{-2} eV^2/

https://doi.org/10.1021/acsomega.1c01890
ACS Omega 2021, 6, 15442−15447

ps, which indicates an ultrafast diffusion in energy space, consistent with the results of Cook et al..[40] Therefore, the simulated results confirmed our speculation about the origin of the hybrid dynamics, that is, the competitive interplay of ultrafast energy diffusion in continuum defect states with ultrafast carrier decay among discrete energy bands. It is worth mentioning that, for the sake of simplicity, in the model, only one defect band has been taken into account. In reality, there exist three discrete defect bands, which may cause the hybrid dynamics to have subtle and quantitative changes.

Based on the satisfactory agreement between experimental observations and our diffusion-controlled relaxation model, we thus confirmed the presence of spectral diffusion in continuum defect bands which became an alternative energy decay channel of photoexcited carriers in highly defective crystals. It is worth mentioning that the absence of spectral diffusion in previous works that deal with defective semiconductors is probably because the defects are not sufficiently dense to form continuum states for energy diffusion to become significant.

CONCLUSIONS

In summary, we have studied the carrier dynamics associated with the defect states in ZnO by TA spectroscopy and observed a hybrid carrier relaxation process with a shoulder feature in the time-domain profile. A Poisson-like dynamics in the time domain was decomposed and attributed to the spectral diffusion in continuum defect bands. A model involving energy diffusion in the energy space has been proposed to qualitatively interpret experimental results. Our results thus suggest that spectral diffusion might be an alternative energy decay channel of carriers in highly defective crystals. This finding may provide new insights into the defect engineering-based performance enhancement of semiconductors.

EXPERIMENTAL SECTION

Materials. Single-crystal ZnO(0001), prepared by the hydrothermal growth technique (MTI Co.), was used as received without further treatment.

Steady-State Absorption Spectroscopy. UV−visible absorption spectroscopy (UV-3700 from Shimadzu) was used in the fine-scan mode with 1 min integration time per 0.01 nm step to verify the defect states in single-crystal ZnO.

TA Spectroscopy. The experimental setup for TA spectroscopy is schematically shown in Figure 1a. Femtosecond laser pulses from Ti: sapphire amplifier (800 nm, 1 kHz, 45 fs) are split into two beams, one of which penetrates a BBO crystal to generate 400 nm pump pulses, while the other passes through a piece of fused silica (4 mm) to produce supercontinuum (SC) probe pulses with a wavelength range of 400−750 nm. Both the pump and probe pulses are then overlapped and focused on the sample with the spot sizes of 0.8 and 0.5 mm, respectively, to minimize excitation inhomogeneity. The time delay between the pump and probe is adjusted by a linear delay stage. The normalized transient transmission spectra $\Delta T_\lambda(t)/T_\lambda(0)$ of the probe pulse, where $\Delta T_\lambda(t) = T_\lambda(t) - T_\lambda(0)$, with $T_\lambda(t)$ and $T_\lambda(0)$ being the probe transmission with and without pumping, respectively, are recorded with a fiber spectrometer (Ocean Optics, FLAME-S-XR1-ES).

AUTHOR INFORMATION

Corresponding Authors

Jau Tang − *Institute of Technological Science, Wuhan University, Wuhan 430072, China*; Email: jautang@yahoo.com

Jianbo Hu − *Laboratory for Shock Wave and Detonation Physics, Institute of Fluid Physics, China Academy of Engineering Physics, Mianyang 621900, China; State Key Laboratory for Environment-Friendly Energy Materials, Southwest University of Science and Technology, Mianyang 621010, China*; orcid.org/0000-0003-2094-0967; Email: jianbo.hu@caep.cn

Authors

Chun Gu − *Laboratory for Shock Wave and Detonation Physics, Institute of Fluid Physics, China Academy of Engineering Physics, Mianyang 621900, China; State Key Laboratory for Environment-Friendly Energy Materials, Southwest University of Science and Technology, Mianyang 621010, China; State Key Laboratory of Advanced Technology for Materials Synthesis and Processing, Wuhan University of Technology, Wuhan 430070, China*

Hang Zhang − *Laboratory for Shock Wave and Detonation Physics, Institute of Fluid Physics, China Academy of Engineering Physics, Mianyang 621900, China; State Key Laboratory for Environment-Friendly Energy Materials, Southwest University of Science and Technology, Mianyang 621010, China*

Yonggang Liu − *State Key Laboratory for Environment-Friendly Energy Materials, Southwest University of Science and Technology, Mianyang 621010, China*

Junhong Yu − *Laboratory for Shock Wave and Detonation Physics, Institute of Fluid Physics, China Academy of Engineering Physics, Mianyang 621900, China*

Junheng Pan − *Institute of Technological Science, Wuhan University, Wuhan 430072, China*

Guoqiang Luo − *State Key Laboratory of Advanced Technology for Materials Synthesis and Processing, Wuhan University of Technology, Wuhan 430070, China*

Qiang Shen − *State Key Laboratory of Advanced Technology for Materials Synthesis and Processing, Wuhan University of Technology, Wuhan 430070, China*

Complete contact information is available at: https://pubs.acs.org/10.1021/acsomega.1c01890

Author Contributions

⊥C.G. and H.Z. contributed equally to this work.

Notes

The authors declare no competing financial interest.

ACKNOWLEDGMENTS

This work was supported by the Science Challenge Project (no. TZ2018001) and Dean Foundation of China Academy of Engineering Physics (No. YZJJLX2017001).

REFERENCES

(1) Queisser, H. J. Defects in Semiconductors: Some Fatal, Some Vital. *Science* **1998**, *281*, 945−950.

(2) McCluskey, M. D.; Haller, E. E. *Dopants and Defects in Semiconductors*, 2nd ed.; CRC Press: Boca Raton, 2018.

(3) Seebauer, E. G.; Noh, K. W. Trends in Semiconductor Defect Engineering at the Nanoscale. *Mater. Sci. Eng., R* **2010**, *70*, 151−168.

(4) McCluskey, M. D.; Janotti, A. Defects in Semiconductors. *J. Appl. Phys.* **2020**, *127*, 190401.
(5) Yu, P. Y.; Cardona, M. Fundamentals of Semiconductors. *Graduate Texts in Physics*; Springer Berlin Heidelberg: Berlin, Heidelberg, 2010.
(6) Feng, J.; Huang, H.; Fang, T.; Wang, X.; Yan, S.; Luo, W.; Yu, T.; Zhao, Y.; Li, Z.; Zou, Z. Defect Engineering in Semiconductors: Manipulating Nonstoichiometric Defects and Understanding Their Impact in Oxynitrides for Solar Energy Conversion. *Adv. Funct. Mater.* **2019**, *29*, 1808389.
(7) Foglia, L.; Vempati, S.; Tanda Bonkano, B.; Gierster, L.; Wolf, M.; Sadofev, S.; Stähler, J. Revealing the Competing Contributions of Charge Carriers, Excitons, and Defects to the Non-Equilibrium Optical Properties of ZnO. *Struct. Dyn.* **2019**, *6*, 034501.
(8) Penfold, T. J.; Szlachetko, J.; Santomauro, F. G.; Britz, A.; Gawelda, W.; Doumy, G.; March, A. M.; Southworth, S. H.; Rittmann, J.; Abela, R.; et al. Revealing Hole Trapping in Zinc Oxide Nanoparticles by Time-Resolved X-Ray Spectroscopy. *Nat. Commun.* **2018**, *9*, 478.
(9) Baldini, E.; Chiodo, L.; Dominguez, A.; Palummo, M.; Moser, S.; Yazdi-Rizi, M.; Auböck, G.; Mallett, B. P. P.; Berger, H.; Magrez, A.; et al. Strongly Bound Excitons in Anatase TiO2 Single Crystals and Nanoparticles. *Nat. Commun.* **2017**, *8*, 13.
(10) Appavoo, K.; Liu, M.; Sfeir, M. Y. Role of Size and Defects in Ultrafast Broadband Emission Dynamics of ZnO Nanostructures. *Appl. Phys. Lett.* **2014**, *104*, 133101.
(11) Li, M.; Xing, G.; Xing, G.; Wu, B.; Wu, T.; Zhang, X.; Sum, T. C. Origin of Green Emission and Charge Trapping Dynamics in ZnO Nanowires. *Phys. Rev. B: Condens. Matter Mater. Phys.* **2013**, *87*, 115309.
(12) Janotti, A.; Van de Walle, C. G. Fundamentals of Zinc Oxide as a Semiconductor. *Rep. Prog. Phys.* **2009**, *72*, 126501.
(13) Tsukazaki, A.; Ohtomo, A.; Onuma, T.; Ohtani, M.; Makino, T.; Sumiya, M.; Ohtani, K.; Chichibu, S. F.; Fuke, S.; Segawa, Y.; et al. Repeated Temperature Modulation Epitaxy for P-Type Doping and Light-Emitting Diode Based on ZnO. *Nat. Mater.* **2004**, *4*, 42−46.
(14) Zhu, H.; Shan, C.; Yao, B.; Li, B.; Zhang, J.; Zhang, Z.; Zhao, D.; Shen, D.; Fan, X.; Lu, Y.; et al. Ultralow-Threshold Laser Realized in Zinc Oxide. *Adv. Mater.* **2009**, *21*, 1613−1617.
(15) Huang, M. H.; Mao, S.; Feick, H.; Yan, H.; Wu, Y.; Kind, H.; Weber, E.; Russo, R.; Yang, P. Room-Temperature Ultraviolet Nanowire Nanolasers. *Science* **2001**, *292*, 1897−1899.
(16) Schifano, R.; Jakiela, R.; Galeckas, A.; Kopalko, K.; Herklotz, F.; Johansen, K. M. H.; Vines, L. Role of Intrinsic and Extrinsic Defects in H Implanted Hydrothermally Grown ZnO. *J. Appl. Phys.* **2019**, *126*, 125707.
(17) Ayaz, S.; Mishra, P.; Sen, S. Structure Correlated Optoelectronic and Electrochemical Properties of Al/Li Modified ZnO. *J. Appl. Phys.* **2019**, *126*, 024302.
(18) Dutta, S.; Chattopadhyay, S.; Sarkar, A.; Chakrabarti, M.; Sanyal, D.; Jana, D. Role of Defects in Tailoring Structural, Electrical and Optical Properties of ZnO. *Prog. Mater. Sci.* **2009**, *54*, 89−136.
(19) Li, D.; Leung, Y. H.; Djurišić, A. B.; Liu, Z. T.; Xie, M. H.; Shi, S. L.; Xu, S. J.; Chan, W. K. Different Origins of Visible Luminescence in ZnO Nanostructures Fabricated by the Chemical and Evaporation Methods. *Appl. Phys. Lett.* **2004**, *85*, 1601−1603.
(20) Zeng, H.; Duan, G.; Li, Y.; Yang, S.; Xu, X.; Cai, W. Blue Luminescence of ZnO Nanoparticles Based on Non-Equilibrium Processes: Defect Origins and Emission Controls. *Adv. Funct. Mater.* **2010**, *20*, 561−572.
(21) Čížek, J.; Valenta, J.; Hruška, P.; Melikhova, O.; Procházka, I.; Novotný, M.; Bulíř, J. Origin of Green Luminescence in Hydrothermally Grown ZnO Single Crystals. *Appl. Phys. Lett.* **2015**, *106*, 251902.
(22) Camarda, P.; Messina, F.; Vaccaro, L.; Agnello, S.; Buscarino, G.; Schneider, R.; Popescu, R.; Gerthsen, D.; Lorenzi, R.; Gelardi, F. M.; et al. Luminescence Mechanisms of Defective ZnO Nanoparticles. *Phys. Chem. Chem. Phys.* **2016**, *18*, 16237−16244.
(23) Kodama, K.; Uchino, T. Thermally Activated Below-Band-Gap Excitation behind Green Photoluminescence in ZnO. *J. Appl. Phys.* **2012**, *111*, 093525.
(24) Djurišić, A. B.; Leung, Y. H.; Tam, K. H.; Hsu, Y. F.; Ding, L.; Ge, W. K.; Zhong, Y. C.; Wong, K. S.; Chan, W. K.; Tam, H. L.; et al. Defect Emissions in ZnO Nanostructures. *Nanotechnology* **2007**, *18*, 095702.
(25) Selim, F. A.; Weber, M. H.; Solodovnikov, D.; Lynn, K. G. Nature of Native Defects in ZnO. *Phys. Rev. Lett.* **2007**, *99*, 085502.
(26) Brauer, G.; Anwand, W.; Grambole, D.; Grenzer, J.; Skorupa, W.; Čížek, J.; Kuriplach, J.; Procházka, I.; Ling, C. C.; So, C. K.; et al. Identification of Zn-Vacancy-Hydrogen Complexes in ZnO Single Crystals: A Challenge to Positron Annihilation Spectroscopy. *Phys. Rev. B: Condens. Matter Mater. Phys.* **2009**, *79*, 115212.
(27) Halliburton, L. E.; Giles, N. C.; Garces, N. Y.; Luo, M.; Xu, C.; Bai, L.; Boatner, L. A. Production of Native Donors in ZnO by Annealing at High Temperature in Zn Vapor. *Appl. Phys. Lett.* **2005**, *87*, 172108.
(28) Lin, B.; Fu, Z.; Jia, Y. Green Luminescent Center in Undoped Zinc Oxide Films Deposited on Silicon Substrates. *Appl. Phys. Lett.* **2001**, *79*, 943−945.
(29) Zubiaga, A.; Plazaola, F.; García, J. A.; Tuomisto, F.; Muñoz-Sanjosé, V.; Tena-Zaera, R. Positron Annihilation Lifetime Spectroscopy of ZnO Bulk Samples. *Phys. Rev. B: Condens. Matter Mater. Phys.* **2007**, *76*, 085202.
(30) Djurišić, A. B.; Choy, W. C. H.; Roy, V. A. L.; Leung, Y. H.; Kwong, C. Y.; Cheah, K. W.; Gundu Rao, T. K.; Chan, W. K.; Fei Lui, H.; Surya, C. Photoluminescence and Electron Paramagnetic Resonance of ZnO Tetrapod Structures. *Adv. Funct. Mater.* **2004**, *14*, 856−864.
(31) Cavaleri, J. J.; Skinner, D. E.; Colombo, D. P.; Bowman, R. M. Femtosecond Study of the Size-Dependent Charge Carrier Dynamics in ZnO Nanocluster Solutions. *J. Chem. Phys.* **1995**, *103*, 5378−5386.
(32) Hu, J.; Vanacore, G. M.; Yang, Z.; Miao, X.; Zewail, A. H. Transient Structures and Possible Limits of Data Recording in Phase-Change Materials. *ACS Nano* **2015**, *9*, 6728−6737.
(33) Fennel, F.; Lochbrunner, S. Förster-Mediated Spectral Diffusion in Disordered Organic Materials. *Phys. Rev. B: Condens. Matter Mater. Phys.* **2012**, *85*, 094203.
(34) Gao, Y.; Talgorn, E.; Aerts, M.; Trinh, M. T.; Schins, J. M.; Houtepen, A. J.; Siebbeles, L. D. A. Enhanced Hot-Carrier Cooling and Ultrafast Spectral Diffusion in Strongly Coupled PbSe Quantum-Dot Solids. *Nano Lett.* **2011**, *11*, 5471−5476.
(35) Tang, J.; Marcus, R. A. Diffusion-Controlled Electron Transfer Processes and Power-Law Statistics of Fluorescence Intermittency of Nanoparticles. *Phys. Rev. Lett.* **2005**, *95*, 107401.
(36) Tang, J.; Marcus, R. A. Single Particle versus Ensemble Average: From Power-Law Intermittency of a Single Quantum Dot to Quasistretched Exponential Fluorescence Decay of an Ensemble. *J. Chem. Phys.* **2005**, *123*, 204511.
(37) Frantsuzov, P.; Kuno, M.; Jankó, B.; Marcus, R. A. Universal Emission Intermittency in Quantum Dots, Nanorods and Nanowires. *Nat. Phys.* **2008**, *4*, 519−522.
(38) Kersting, R.; Lemmer, U.; Mahrt, R. F.; Leo, K.; Kurz, H.; Bässler, H.; Göbel, E. O. Femtosecond Energy Relaxation in π-Conjugated Polymers. *Phys. Rev. Lett.* **1993**, *70*, 3820−3823.
(39) Scheblykin, I. G.; Yartsev, A.; Pullerits, T.; Gulbinas, V.; Sundström, V. Excited State and Charge Photogeneration Dynamics in Conjugated Polymers. *J. Phys. Chem. B* **2007**, *111*, 6303−6321.
(40) Cook, C. J.; Khan, S.; Sanders, G. D.; Wang, X.; Reitze, D. H.; Jho, Y. D.; Heo, Y.-W.; Erie, J.-M.; Norton, D. P.; Stanton, C. J. Ultrafast Carrier Relaxation and Diffusion Dynamics in ZnO. In *Oxide-Based Materials and Devices*; Teherani, F. H., Look, D. C., Litton, C. W., Rogers, D. J., Eds.; SPIE, 2010; Vol. *7603*, p 760304.

https://doi.org/10.1021/acsomega.1c01890
ACS Omega 2021, 6, 15442−15447